15th_Paper_Nurhasni_Hasan_IJBM_(2019).pdf

by

Submission date: 04-Apr-2023 03:37PM (UTC+0700)
Submission ID: 2055485736
File name: 15th_Paper_Nurhasni_Hasan_IJBM_(2019).pdf (3.98M)
Word count: 10022
Character count: 53021

International Journal of Biological Macromolecules 142 (2020) 680–692

Contents lists available at ScienceDirect

International Journal of Biological Macromolecules

journal homepage: www.elsevier.com/locate/ijbiomac

Chitosan-based nitric oxide-releasing dressing for anti-biofilm and *in vivo* healing activities in MRSA biofilm-infected wounds

Moonjeong Choi [1], Nurhasni Hasan [1], Jiafu Cao, Juho Lee, Shwe Phyu Hlaing, Jin-Wook Yoo *

College of Pharmacy, Pusan National University, Busan 609-735, South Korea

ARTICLE INFO

Article history:
Received 8 July 2019
Received in revised form 19 September 2019
Accepted 1 October 2019
Available online 14 October 2019

Keywords:
Chitosan dressing
Nitric oxide-releasing system
MRSA biofilm-infected wound healing

ABSTRACT

Bacterial biofilms on wounds impair the healing process and often lead to chronic wounds. Chitosan is a well-known biopolymer with antimicrobial and anti-biofilm effects. S-nitrosoglutathione (GSNO) has been identified as a promising nitric oxide (NO) donor to defend against pathogenic biofilms and enhance wound healing activities. In this study, we prepared NO-releasing chitosan film (CS/NO film) and evaluated its anti-biofilm activity and *in vivo* wound healing efficacy against methicillin-resistant *Staphylococcus aureus* (MRSA) biofilm-infected wounds in diabetic mice. The *in vitro* release study showed sustained release of NO over 3 days in simulated wound fluid. The CS/NO film significantly enhanced antibacterial activity against MRSA by > 3 logs reduction in bacterial viability. Moreover, CS/NO film exhibited a 3-fold higher anti-biofilm activity than the control and CS film. In *in vivo* MRSA biofilm-infected wounds, the CS/NO film-treated group showed faster biofilm dispersal, wound size reduction, epithelialization rates, and collagen deposition than the untreated and CS film-treated groups. Therefore, the CS/NO film investigated in this study could be a promising approach for the treatment of MRSA biofilm-infected wounds.

© 2019 Elsevier B.V. All rights reserved.

1. Introduction

Wound healing is a complex process that requires the collaborative efforts of many different tissues and cell lineages to accelerate the healing for wound closure [1]. Wound healing includes overlapping phases, starting from the formation of a blood clot and inflammation, followed by proliferation and migration of dermal and epidermal cells. Further, matrix synthesis occurs to fill the wound gap and reestablish the skin barrier. Finally, tissue remodeling and differentiation lead to complete recovery of the skin tissue and restoration of skin aesthetics [2].

However, Wound healing is often delayed by bacterial infections that can cause tissue necrosis and systemic infection [3]. Once the skin is injured, microorganisms that are normally sequestered on the skin surface obtain access to the underlying tissues. Both bacteria and endotoxins can lead to the prolonged elevation of pro-inflammatory cytokines and elongate the inflammatory phase. If this process continues, the wound enters a chronic wound state, e.g., diabetic foot ulcer and gangrene [4–6]. Under these conditions, bacteria in the wounds can form biofilms, i.e., complex communities of surface-attached bacteria embedded in a self-secreted extracellular polymeric substance (EPS). Mature biofilms develop protected microenvironments, which shield bacteria from the phagocytic activity of invading polymorphonuclear neutrophils, increasing their resistance to conventional antibiotics [6,7]. The cases of bacterial infections in the form of biofilm-infected wounds increased over the past decade, and have led to significant mortality and morbidity [8].

Biofilm-infected wounds are commonly caused by staphylococci, such as *Staphylococcus epidermidis* and *Staphylococcus aureus* [9]. Methicillin-resistant *Staphylococcus aureus* (MRSA) is a major nosocomial pathogen that has emerged as a dire problem in cases of diabetic foot ulcer, which, unless properly treated, results in amputation [10–12]. Therefore, there is an urgent need for effective therapies for the treatment of MRSA biofilm-infected wounds.

The current treatment strategies for MRSA biofilm-infected wounds include physical intervention and antimicrobial agents such as antibiotics, antiseptics, iodine and ionic silver [13]. However, these strategies fail to suppress biofilms, and there is a growing concern related to antibiotic resistance [14,15]. Furthermore, for the complete treatment of biofilm-infected wounds, treatment strategies should be able to kill bacteria, disperse the biofilm, and trigger wound repair via cell proliferation and tissue remodeling. In this regard, there is a need for effective treatment options for MRSA

* Corresponding author.
E-mail address: jinwook@pusan.ac.kr (J.-W. Yoo).
[1] Both these authors contributed equally to this work.

https://doi.org/10.1016/j.ijbiomac.2019.10.009
0141-8130/© 2019 Elsevier B.V. All rights reserved.

biofilm-infected wounds that possess these three activities simultaneously (i.e., anti-biofilm, antibacterial, and wound repair).

Nitric oxide (NO) has recently emerged as a promising therapeutic agent for antibacterial, anti-biofilm and wound healing activities. NO is a diatomic free radical that is endogenously generated by NO synthases via the five-electron oxidation of the amino acid L-arginine [16]. NO has a potent antibacterial activity against MRSA [2] causing the damage and lysis of cell wall [17]. Importantly, it has been also reported that NO can prevent biofilm formation and disperse established biofilm through the intracellular second messenger cyclic di-GMP, which can initiate a range of effector functions and trigger biofilm dispersal [18]. As for the MRSA biofilm, the reactive nitrogen species derived from NO and superoxide ($O_2^{\cdot-}$) act by downregulating the production of polysaccharide intercellular adhesion which is a pivotal material for the development of strong substrate attachment of MRSA cells to the surface to form biofilm [19]. Furthermore, NO accelerates wound healing processes by regulating cell proliferation, wound contraction, and collagen formation [20,21].

Despite the beneficial properties of NO, its therapeutic applications are restricted due to its gaseous property and extremely short half-life (3–4 s), which necessitates a delivery system that can control its storage and release. To overcome the limitations of NO as a therapeutic agent, various NO delivery systems, such as hydrogels, ointment, and micro/nanoparticles have been developed to control the storage and release of NO [17,22–25]. For wound treatments, film-type dressings have been extensively studied due to their ability to maintain a moist environment that facilitates wound healing. In this regard, our group previously developed the NO-releasing chitosan film (CS/NO film) using S-nitrosoglutathione (GSNO), a naturally occurring NO donor that can be applied topically as a wound dressing for antibacterial and wound healing effects, and chitosan (CS) as a film-forming polymer [26]. CS is a well-known biocompatible and biodegradable polysaccharide biopolymer which exhibits unique polycationic, chelating, and film-forming properties as well as antibacterial, hemostatic, wound healing, and mucoadhesive activities; thus, it has been used in various drug delivery systems [27–32]. Also, CS is known to have a low toxicity to mammalian cells [33,34]. More importantly, a recent study demonstrated that CS has anti-biofilm activity against biofilm-related recalcitrant MRSA infections [35].

In our previous study, we developed CS/NO films and examined their antibacterial activity against non-antibiotic resistant gram positive and gram negative bacteria and wound healing effect to non-infected full-thickness wounds [26]. The aim of the current study was to evaluate the synergistic effect of CS and GSNO in the CS/NO film for the treatment of MRSA biofilm-infected wounds. We evaluated the *in vitro* release profile using simulated wound fluid (SWF), which mimics the actual wound condition. The *in vitro* anti-biofilm activity of the CS/NO film against MRSA biofilm was also determined. *In vivo* anti-biofilm and wound healing activities were evaluated using a mouse model of MRSA biofilm-infected wounds under the diabetic condition.

2. Materials and methods

2.1. Materials

CS (low-molecular-weight: 50–190 kDa, viscosity: 20–300 cps; acetylation: 75–85%), sodium nitrite, reduced L-glutathione, sodium acetate, crystal violet, streptozotocin (STZ), tetramethylrhodamine isothiocyanate (TRITC), Mayer's hematoxylin, eosin-Y disodium, 2,2,2-tribromoethanol and *tert*-amyl alcohol (2-methyl-2-butanol) (Avertin anesthesia component), 5% glutaraldehyde, tetrazolium dye 3-(4,5-di-methylthiazol-2-yl)-2,5-diphenyltetrazolium bromide (MTT), and dimethylsulfoxide (DMSO) were purchased from Sigma-Aldrich (St. Louis, MO, USA). Bacto™ Tryptic Soy Broth (TSB) and peptone were purchased from BD Biosciences (Sparks, MD, USA). The LIVE/DEAD® Baclight™ bacterial viability kit (Molecular Probes) were purchased from Life Technologies (Eugene, OR, USA). Further the Dulbecco' Modified Eagle Medium (DMEM) medium, trypsin, fetal bovine serum (FBS), and penicillin–streptomycin was purchased from Hyclone, Thermo Fisher Scientific Inc. (Waltham, MA, USA). Masson's trichrome (MT) stain was purchased from Abcam (Cambridge, MA, USA). Polyurethane coupon (high-temperature polymer) was purchased from BioSurface Technologies Corporation (Bozeman, MT, USA). Adhesive tape (Micropore) and Tegaderm™ (transparent dressing) were purchased from 3 M Health Care (St Paul, MN, USA). Phosphate buffered saline (PBS; 20 ×) was purchased from Biosesang (Seoul, Republic of Korea). All other reagents and solvents were of analytical grade.

2.2. Synthesis of GSNO

GSNO was synthesized as described previously [36]. In brief, reduced L-glutathione was dissolved in 2 M HCl at 4 °C. Sodium nitrate was added, and the mixture was placed in an ice bath under stirring for 40 min. The final solution was precipitated with cold 80% acetone and stirred for another 20 min. The precipitation was collected and washed once with cold 80% acetone, twice with cold 100% acetone, and thrice with cold diethyl ether. The final GSNO powder was freeze-dried and stored at − 20 °C until further use.

2.3. Preparation of the CS/NO film

The CS/NO film was prepared as described previously with some modifications (Fig. 1A) [26]. In brief, CS was dissolved in 0.1 M acetate buffer solution (pH 4.4) to prepare CS solution (1 w/v%). Glycerol as a plasticizer was added to the CS solution at a final concentration of 1 wt%. Various amounts of GSNO (5, 10 and 20 wt%) were added to 20 g of the CS solution. The final solution was poured into a petri dish and dried at 30 °C for 12 h in an incubator with a dehumidifier to accelerate solvent evaporation. A CS film without addition of GSNO was prepared using the same procedure. The resulting films were stored at 4 °C in a desiccator under dark condition until use.

2.4. In vitro NO release in SWF

The release of NO from the 20% CS/NO film was examined in SWF (pH 7.0). SWF comprises 0.1 g of peptone and 0.85 g of NaCl in 100 mL of distilled water mixed with FBS at a ratio of 1:1 [37]. The 20% CS/NO films were cut into squares equivalent to the weight of 100 mg and added to 0.12 mL (100% swollen condition) and 0.6 mL (500% immersed condition) of SWF to mimic the natural swollen and immersed conditions, respectively [26]. Samples were incubated at 37 °C for 1, 4, 8, 12, 24, 48, and 72 h. At predetermined time intervals, the remaining 20% CS/NO films with SWF were dissolved in 0.1 M cold HCl to measure residual GSNO concentration. Then, samples were centrifuged at 20,000*g* for 10 min to remove insoluble matters and the clear supernatant was analyzed using a spectrophotometer (Optizen 2120 UV, Mecasys, Republic of Korea) at a wavelength of 330 nm. The concentration of NO released from the film at time t ([*NO*]t) can be calculated from the known concentration of GSNO.

$$[NO]t = [GSNO]0 - [GSNO]t$$

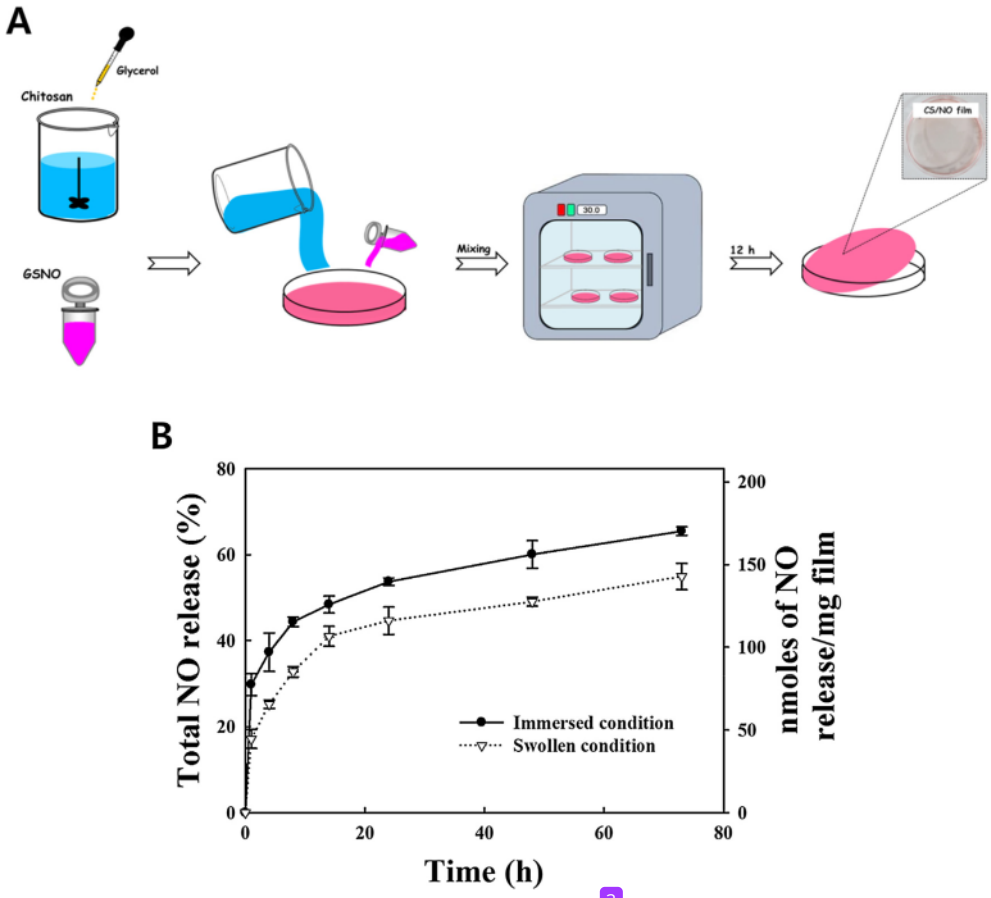

Fig. 1. (A) Preparation of the CS/NO film. (B) *In vitro* NO release from the 20% CS/NO film in SWF. The CS/NO films were placed in SWF (pH 7.0) under the swollen and immersed conditions at 37 °C. Values are expressed as mean ± SD (n = 3).

where $[GSNO]_0$ is the initial concentration of GSNO and $[GSNO]_t$ is the concentration of GSNO at time t. The amount of NO was determined based on the equation below:

$$GSNO\ (1\ \ mol) \rightarrow GSH + NO\ (1\ \ mol)$$

2.5. In vitro antibacterial activity

The bacterial strain used in this study was MRSA (USA300) FPR3757 (GenBank accession no.: NC_00793). The bacteria were cultured in TSB medium (in 1 L of TSB medium consist of 17 g pancreatic digest of casein, 3 g papaic digest of soybean, 2.5 g dextrose, 5 g sodium chloride and 2.5 g dipotassium phosphate) at 37 °C for 15 h on an orbital shaker (100 rpm) and grown up to the mid-exponential phase. The resulting bacterial suspension was centrifuged at 1000 × *g* for 15 min. The pellet was re-suspended in sterile PBS and adjusted to an appropriate concentration. A total of 100 μL of MRSA suspension [final concentrations: 10^{10} colony-forming unit (CFU)/mL] was incubated with 1.9 mL of TSB medium. Then, pieces (15 mg) of the CS/NO film concentrations of 5%, 10%, and 20% were placed in 12-well plates. A well without film was used as a control. All samples were incubated at 37 °C for 24 h in a shaking incubator; then, they were centrifuged at 8000 × *g* and washed twice with 0.85% NaCl.

For the assessment of bacterial viability (CFU measurement), after serial dilution, a 200 μL aliquot of each dilution was plated on TSB agar medium and incubated at 37 °C overnight. Then, the number of colonies was enumerated, factoring in the number of viable bacteria at the time of plating. For the confocal study, bacterial suspensions were stained with the LIVE/DEAD® Baclight™ bacterial viability kit reagents according to the manufacturer's protocol. The samples were observed with the FluoView FV10i confocal microscope to differentiate live bacteria from the dead ones. Bacteria stained green with SYTO-9 at excitation (Ex)/emission (Em) wavelengths of 539/570–620 nm were considered viable/live and those stained red with propidium iodide (PI) at Ex/Em 470/490–540 nm were considered dead.

2.6. In vitro anti-biofilm activity

MRSA (USA300) FPR3757 suspensions were prepared as described above. A total of 200 μL of the MRSA suspension (final concentration 10^{10} CFU/mL) was placed on the surface of polyurethane coupon (BioSurface Technologies Corporation, Bozeman, MT) and incubated at 37 °C for 8 h to facilitate biofilm formation. Then, pieces of the CS/NO films (15 mg) were placed on the surface of the biofilm-covered polyurethane coupon with 1.8 mL of TSB medium. Coupons without the CS or CS/NO films were used as

controls. All samples were then incubated at 37 °C for 24, 48 and 72 h. After incubation, the remaining CS/NO films were removed, and the biofilm of the coupons was washed with PBS. One milliliter of 0.1% crystal violet was added, and the coupons were incubated in the dark for 20 min, followed by washing with PBS. Quantitative analysis of the remaining crystal violet biofilm was performed by adding 1 mL of 100% ethanol; then, 200 μL of solution from each well was transferred to a 96-well plate, and the optical density (OD) of the crystal violet present was measured at a wavelength of 550 nm.

2.7. In vitro cytotoxicity study

L929 mouse fibroblast cells were obtained from the Korean Cell Line Bank (Seoul, Republic of Korea). Cells were grown to subconfluency in DMEM with 10% (*v*/*v*) FBS supplemented with antibiotics (100 μg/mL streptomycin sulfate and 100 IU/mL penicillin G sodium). The cells were trypsinized, suspended in media at concentration of 5×10^4 cells per well, and then plated onto 96-well plates. After 48 h incubation, the medium from each well was replaced with fresh media (100 μL) containing the supernatant from the film-media mixture (each film was put into the complete medium for 48 h) at various concentrations (10, 100, 1,000, and 10,000 μg/mL). After 24 h incubation, a standard MTT viability assay was performed. MTT solution in sterile PBS was mixed to each well and the incubation was continued for 2 h. After that, all solution was then removed from the well and 150 μL DMSO was added to solubilize the crystals. The absorbance measured at 540 nm was comparable to the concentration of viable cells in every well. The untreated cells were used as control. The data were expressed as mean ± standard deviation of eight replicates (n = 8). The fibroblast viability was determined using equation below:

$$\text{Cell viability}(\%) = \frac{Absorbance\ (treated\ cells)}{Absorbance\ (control\ cells)} \times 100$$

2.8. In vivo biofilm formation

All animal experiments were performed in accordance with the regulations of Pusan National University and Korean legislation on animal studies. MRSA (USA300) FPR3757 was used to develop an *in vivo* biofilm on the wound. The bacteria were cultured in TSB medium at 37 °C overnight on an orbital shaker (100 rpm) and grown up to the mid-exponential phase (10^7 CFU/mL). The resulting bacterial suspension (final concentration: 10^9 CFU/mL) was centrifuged 8000 × *g* for 15 min at. The pellet was re-suspended in TSB medium and adjusted to an appropriate concentration. A total of 6 μL of MRSA suspension (final concentration 10^9 CFU/mL) was placed on the surface of the wound and covered with a membrane filter that had been dipped in MRSA suspension. Then, the bacterial infected wound was covered with Tegaderm™ (transparent dressing; 3 M Health Care, St. Paul, MN, USA) for 72 h for biofilm formation.

2.9. Confirmation of in vivo biofilm

To confirm biofilm formation on the wound, scanning electron microscopy (SEM) and confocal microscopy were performed. The *in vivo* biofilm was cut through the central part of the wound. For SEM, samples were treated as previously reported [38]. The biopsies were fixed in 2.5% glutaraldehyde solution (pH 7.2) at 4 °C overnight. Then, they were rinsed twice in PBS and dehydrated in a graded series of ethanol (50%, 70%, 80% and 100%; application time: 10 min); next, the samples were mounted on double-sided carbon tape and dried in a vacuum dryer overnight. Prior to observation, the samples were spray-coated with platinum for 2 min under vacuum. Then, the samples were viewed under the Carl Zeiss SUPRA25 & Raith Quantum Elphy E-beam lithography system and Zeiss SEM (Carl Zeiss, Germany) at an accelerating voltage of 2.0 kV.

For confocal microscopy, the fixed biofilm with 2.5% glutaraldehyde solution were washed once with PBS and twice with 0.85% NaCl. Then, SYTO 9 and TRITC dye (Ex/Em; 557/576) were added, and the samples were incubated at room temperature for 90 min. Cells were washed with PBS and transferred onto slides. Biofilms or adhered cells were observed with the FluoView FV10i confocal microscope.

2.10. Induction of diabetes

STZ is widely used to induce insulin-dependent diabetes mellitus, also known as type-1 diabetes mellitus [39]. Food was completely removed from animal cages 4 h prior to STZ injection. STZ (40 mg/kg) was dissolved in 50 mM sodium citrate buffer solution (pH 4.5) to a final concentration of 6 mg/mL. The STZ solution was intraperitoneally (i.p) injected into mice on 5 consecutive days. The mice with fasting blood glucose levels above 300 mg/dL were used as diabetic models.

2.11. In vivo wound-healing assay

To evaluate the *in vivo* wound healing efficacy of the CS/NO film, male ICR mice (7 weeks, weight 30–35 g; Samtako Bio Korea) were used as an animal model. Prior to the development of wounds on the dorsal area, the mice were anesthetized i.p using avertin. Dorsal hair was shaved with an electric razor and hair removal cream (Veet, Reckitt Benckiser). Subsequently, back skin was excised using a 6-mm biopsy punch to create full-thickness wounds. The wound models were divided into two groups: biofilm-challenged non-diabetic and diabetic mice. For biofilm induction, the wounds were treated as described in Section 2.8. CS or CS/NO film (0.8 cm × 0.8 cm, 15 mg) was applied topically to each wound from day 3 post-injury. Untreated mice were used as the control group. All films were covered again with Tegaderm™ (transparent dressing; 3 M Health Care, St. Paul, MN) to represent splint model and then fixed with tape. Dressings on wounds were replaced with new dressings every 3 days. Digital images of the wounds were taken every 3 days to observe visual wound healing. Adobe Acrobat 9 Professional was used to determine wound size reduction and calculated as follows:

$$\text{Woundsizereduction} = \frac{Wt}{Wo} \times 100$$

where W_0 is the wound area at initial time 0, and W_t is the wound area at time t.

2.12. Histological processing of the wound area

Cross-sectional full-thickness skin specimens and deep granulation tissues were collected on the last day of the *in vivo* experiment. Full wound areas were excised, fixed in 10% formaldehyde for 24 h and blocked with paraffin. After the samples were embedded in paraffin, histological sections were cut (2 μm) from paraffin-embedded fixed tissues using a microtome. Histological samples were fixed to glass slides and stained with hematoxylin and eosin (H&E) and Masson's trichrome (MT) stain to evaluate skin morphology and collagen formation, respectively. The slides were analyzed by light microscopy (Olympus BX53) and images were digitally captured at a resolution of 1360 × 1024 pixels with an Olympus DP70 digital camera.

2.13. Reduction of wound bacterial burden

Bacterial burden (bacterial viability) in the wounds was examined at day 9 and 15 post-injury in the non-diabetic and diabetic groups. After examining the wounds on the respective days, wound skin tissues were recovered, and the skin lesion tissues with biofilm were homogenized in sterile PBS and cultured onto TSB agar at 37 °C overnight. The number of colonies was counted, factoring in the number of viable bacteria at the time of plating.

2.14. Statistical analysis

Statistical analysis was performed using one-way analysis of variance followed by Tukey's multiple comparison test or unpaired *t*-test in GraphPad Prism 5.0 (GraphPad Software, La Jolla, California). In cases of significant deviations from *t*-test, nonparametric Mann–Whitney *U*-test was conducted to compare the distributions of two unpaired groups. A value of $P < 0.05$ was considered statistically significant. Data are presented as mean ± SD.

3. Results and discussion

3.1. In vitro NO release profile of the CS/NO film in SWF

The preparation and characterization of the CS/NO film (Fig. 1A) have been reported in our previous study [26]. CS/NO film has a reddish, transparent and homogenous surface. The amount of NO loading in the CS/NO film was 0.26 μmoles/mg film (Table 1). Because the aim of the current study was to evaluate the efficacy of the CS/NO film dressing for the treatment of MRSA biofilm-infected wounds under the diabetic condition, we first measured *in vitro* NO release from the CS/NO film to determine the frequency of the CS/NO/film application on wound. Due to the diverse components of wound fluids that can affect the release of NO from the CS/NO film [40], *in vitro* NO release was tested in SWF as a release medium under the immersed and swollen conditions, which mimic the actual wound conditions. The swollen condition represents wounds with a low amount of exudate in which the CS/NO film swells slowly, absorbs exudate, and causes slow NO release, whereas the immersed condition represents wounds with a high amount of exudate in which the CS/NO film swells rapidly, causing slightly faster NO release.

As shown in Fig. 1B, NO release from the CS/NO film in the first 1 h were 17.1% and 29.8% under the swollen and immersed conditions, respectively. After the initial fast release, NO was released slowly from CS/NO film over 3 days. In detail, the CS/NO film released 49.1% (127.6 nmoles NO/mg film) and 60.1% (156.2 nmoles NO/mg film) of NO at day 2 under the swollen and immersed conditions, respectively. The CS/NO film continued to release < 80% of NO up to day 3 under both swollen (released 54.9%, 142.8 nmoles/mg film) and immersed conditions (released 65.5%, 170.2 nmoles/mg film). In this regard, the sustained NO release was best represented by the hydrated film under the swollen condition. The slow release can be attributed to the required time in which the film absorbs water to swell and release the entrapped drug [26]. The dual NO release patterns observed in this study are beneficial, the fast release facilitates dispersal of MRSA biofilm, whereas the sustained release assists in the maintenance of a sufficient NO concentration at the wound site to accelerate wound repair (i.e., eradication of planktonic bacteria, proliferation, and wound tissue remodeling) [17,41]. We also found that the amount of released NO was still released < 80% up to day 3 under both swollen and immersed conditions, suggesting that the CS/NO film can release NO during wound treatment, which also lowers the frequency of CS/NO film application on wound (i.e., every 3 days).

Table 1
Characterization of CS and CS/NO films.

Films	NO amount (μmoles/mg films)	Thickness (μm)	Physical characteristics
CS	Not determined	68 ± 6	Transparent and homogenous surface
CS/NO	0.26 ± 0.006	69 ± 5	Reddish, transparent and homogenous surface

Values are expressed as mean ± SD of three different batches of films.

3.2. In vitro antibacterial activity

Prior to evaluation of the effectiveness of the CS/NO film in dispersing biofilm and accelerating wound healing in *in vivo* MRSA biofilm-infected wounds, the *in vitro* antibacterial activity against MRSA was evaluated by confocal microscopy and CFU measurement. Untreated bacteria were used as controls. Since, CS is a biodegradable polymer with proven antimicrobial activity against gram positive and gram negative bacteria [42–45], the antibacterial activity of the CS film was investigated. In this study, we hypothesized that the combination effect of CS and GSNO improves the efficacy the CS/NO film for the treatment of MRSA biofilm-infected wounds.

A reduction in MRSA viability was observed by distinguishing live and dead bacteria using confocal microscopy (Fig. 2A). The live and dead reagents stained live cells represented by green fluorescence (SYTO-9) and dead cells were represented by red fluorescence (PI). SYTO-9 penetrates all bacterial membranes, whereas PI only penetrates cells with damaged membranes [46]. The CS film showed a slight antibacterial effect against MRSA, whereas the CS/NO film showed significant concentration-dependent antibacterial activity. As the GSNO concentration increased in the CS/NO film, the population of live bacteria decreased and that of dead bacteria increased. Overall, significant antibacterial activity against MRSA was observed with the 20% CS/NO film compared with the CS film and untreated controls. Furthermore, we performed the CFU study to confirm the ability of the CS/NO film in reducing MRSA viability. As shown in Fig. 2B, similar to the results obtained on confocal microscopy, the CS film revealed a slight anti-MRSA effect by reducing the bacterial viability by < 1 log. In contrast, the 20% CS/NO film (2.1 μmoles of NO) reduced bacterial viability by > 3 logs (~99.9% of killing) against MRSA. A reduction of bacterial viability by > 1 log (~90% of killing) and > 2 logs (~99% killing) against MRSA was observed with the 5% CS/NO film (0.3μmoles of NO) and 10% CS/NO film (1 μmoles of NO), respectively. These results were in line with the macroscopic images of bacterial density in TSB medium, which also indicated that 20% CS/NO film significantly killed bacteria (Fig. 2C), compared with the CS film as well as the 5% and 10% CS/NO films. Thus, these results suggest that the 20% CS/NO films have potent antibacterial activity against MRSA. Based on the results, the 20% CS/NO film was chosen for further studies.

The enhanced antibacterial effect of the CS/NO film can be attributed to combined mechanisms of CS and NO in killing bacteria, wherein they complement each other. CS can kill MRSA by interacting with the bacterial cell membrane, resulting in mutations in cell wall permeability and exposure of intracellular compounds [47]. NO has multiple antibacterial mechanisms of action. The superoxide (O_2^-) and reactive nitrogen species procured from NO enable cell wall lysis and modification of proteins, lipids, and DNA as well as kill MRSA indirectly by modifying the immune response or different host cell function. In addition, GSNO is known

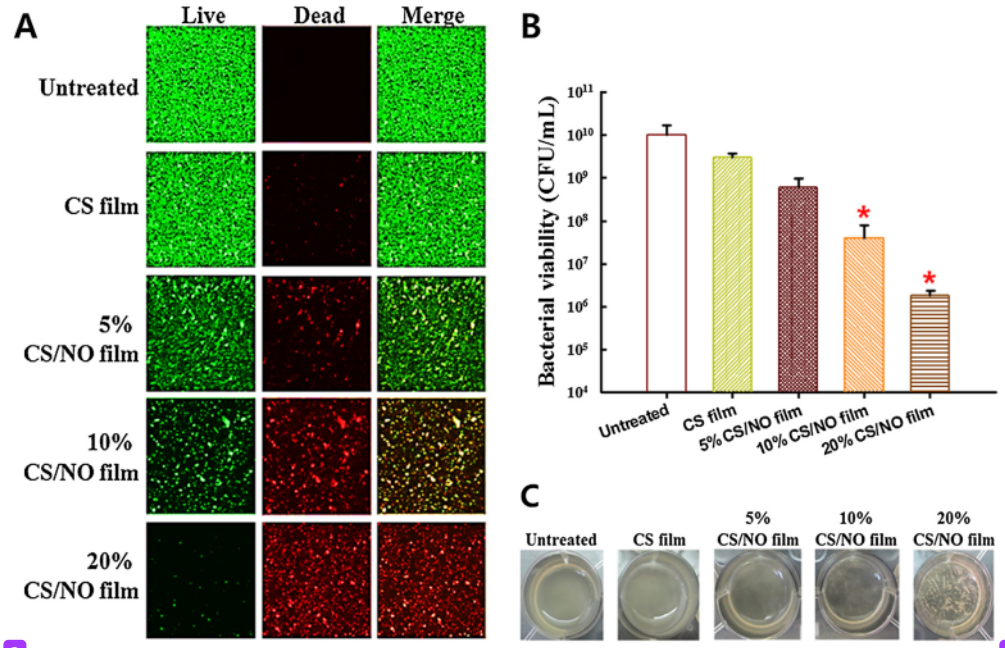

Fig. 2. *In vitro* antibacterial activities of the CS film and CS/NO film against MRSA. (A) Confocal microscopy images of MRSA biofilm after 24 h treatment with the CS/NO film at different concentrations. (B) Bacterial viability (CFU measurement). Values are expressed as mean ± SD (n = 3); *P < 0.05 compared with the untreated group. (C) Macroscopic images of bacterial density in TSB medium.

as the most effective biological *trans*-nitrosating agent that kills bacterial cells by nitrosation of their cellular proteins [17,48]. Although, in this study, the antibacterial activity of the CS film did not meet the standard of significant anti-MRSA effect, it is worth noting that the antibacterial activities of chitosan vary depending on the degree of deacetylation, polymerization, zeta potential, pH value, and molecular weight [47,49]. Nevertheless, the combination of CS and NO in CS/NO film significantly increased its antibacterial activity and prevented the growth of bacteria. Many studies have reported that the combination of CS with antibiotics enhances antibacterial activity [50–53]. Furthermore, the biodegradability, biocompatibility, and antibacterial properties of CS are preferable properties for wound dressing-based materials compared with those of synthetic polymers [54].

3.3. In vitro anti-biofilm activity

Next, we tested the efficacy of the film to disperse the *in vitro* MRSA biofilm using crystal violet staining. A bacterial infection in the form of a biofilm on the surface of a wound represents a significant hindrance in wound repair. The strong biofilm and uncontrolled growth of planktonic bacteria within biofilm biomass can cause the infection to infiltrate deep wound tissues and impede the processes involved in wound healing ranging from angiogenesis to re-epithelialization [55]. Therefore, the dispersal of biofilm on the wound and eradication of planktonic bacteria play pivotal roles in efficient wound healing. The biological properties of biofilms have been represented by their viable biomass and EPS levels [56]. Crystal violet measures the total biofilm biomass, including bacterial cells and EPS matrix [57]. As discussed above, further analysis was conducted using the 20% CS/NO film (hereafter called CS/NO film). Based on the facts that CS possesses anti-biofilm activity against MRSA [58] and NO is a key mediator of biofilm dispersal [59], we hypothesized that the combination of CS and NO in the form of wound dressing enhances the anti-biofilm effect.

The *in vitro* anti-biofilm activities of the CS and CS/NO films at different incubation times (24, 48, and 72 h) are shown in Fig. 3A and B. Biofilm attachment to polyurethane coupon is shown in purple, stained by crystal violet. As shown in Fig. 3A, biofilm treated with the CS and CS/NO films showed time–dependent biofilm dispersal and a greater biofilm dispersal effect was observed within 72 h than in the control (coupon without film). The CS/NO film revealed more prominent biofilm dispersal than the CS film shown by the faded purple color on polyurethane coupon. This can be attributed to the combined anti-biofilm effects of CS and NO. CS with other polysaccharides have been reported to act as signaling molecules that contribute to the modulation of the gene expression of recipient bacteria, resulting in biofilm dispersal or triggering cell motility for the disintegration of planktonic bacteria within biofilm biomass [60,61]. The anti-biofilm activity of NO is attributed to the reactive byproducts of NO, which act by downregulating the production of polysaccharide intracellular adhesion, i.e., the homopolymer contributes to the development of a strong substrate attachment [19]. The macroscopic observation of biofilm dispersal on polyurethane coupon was followed by the quantification of the biofilm biomass absorption spectrum observed at OD_{550}. The reduction in biofilm mass of the CS and CS/NO films (2.1 μmoles of NO) at 24 h was 15.0% and 41.3%, respectively. After 48 h incubation, the reduction in biofilm mass was 38.5% and 59.0% for the CS and CS/NO films (2.3 μmoles of NO), respectively. Consistent with the macroscopic images obtained with crystal violet staining (Fig. 3A), the reduction in biofilm mass was more significant after 72 h incubation time than that after 24 and 48 h incubations, which showed OD_{550} values of 48.3% for the CS film and 85.6% for the CS/NO film (2.5 μmoles of NO) (Fig. 3B). Overall, compared with the untreated group (control) and CS film, the CS/NO film exhibited a superior biofilm dispersal effect. The significant

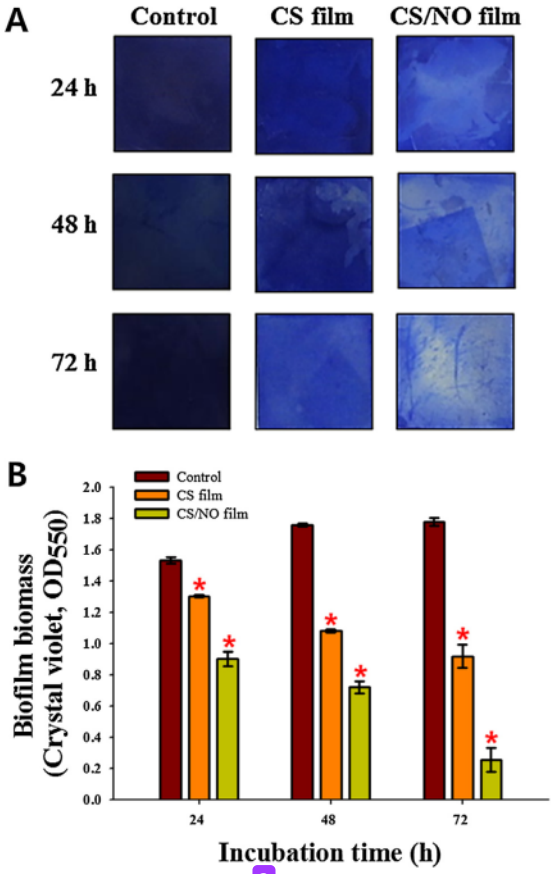

Fig. 3. *In vitro* anti-biofilm activity of the CS and CS/NO films. MRSA biofilms were grown in polyurethane coupon for up to 24 h in the presence/absence of CS or CS/NO. (A) Stained biofilms on coupon by crystal violet. (B) Biofilm biomass by crystal violet staining (OD_{550}). Values are mean ± SD (n = 3); *P < 0.05 compared with the untreated group.

anti-biofilm effect of the CS/NO film was related to NO release profile shown in Fig. 1. NO was released in a sustained manner for over 3 days, which agrees with the time (72 h) required for prominent biofilm dispersal, as discussed above. Taken together, these results demonstrate that the combination of CS and NO in the form of film provides synergistic effects on biofilm dispersal.

3.4. In vitro cytotoxicity study

Cytotoxicity of CS film and CS/NO film was evaluated using healthy L929 mammalian fibroblast cells which are a suitable cell line for *in vitro* cytotoxicity study due to their significant role in wound healing, epithelial-mesenchymal interaction, and the development of the extracellular matrix [62]. As shown in Fig. 4 CS film and CS/NO film did not show any significant cytotoxicity (>87% viability) to L929 fibroblast cells regardless of their concentrations, implying that CS and NO released from film are safe for topical application.

3.5. Biofilm characterization of in vivo biofilm

To evaluate the wound healing efficacy of the CS/NO film against biofilm challenge, we prepared an *in vivo* MRSA biofilm

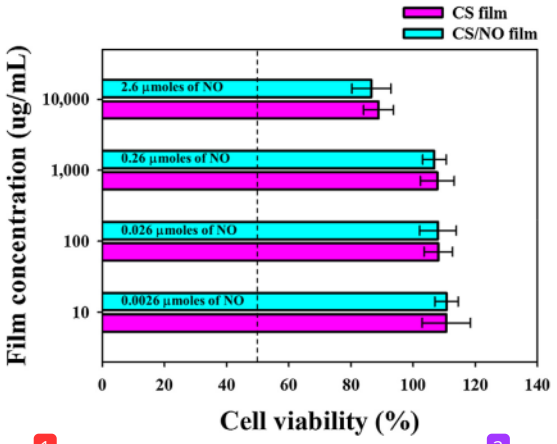

Fig. 4. Viability (%) of L929 mouse fibroblast cells after 24 h exposure to CS film and CS/NO film at various concentration (n = 8).

on wounds in mice models. Biofilms are primarily composed of microbial cells and EPS, which is composed of polysaccharides and proteins. EPS is the construction material of bacterial biofilm formation and either remains attached to a cell's outer surface or is secreted into its growth medium. Planktonic MRSA is recognizable as individual bacteria. The formation of bacterial biofilm proceeds in two phases: primary attachment of bacteria cells on a wound followed by bacterial accumulation in multiple layers and glycocalyx formation leading to the formation of a mature biofilm [63]. Biofilms were formed on the surfaces of wound tissues after 3 days incubation with ~ 10^9 CFU/mL of MRSA suspension (Fig. 5A). To confirm biofilm formation on a wound, an *in vivo* biofilm was cut through the central part of the wound and observed by SEM and confocal microscopy. SEM image of the *in vivo* MRSA biofilm showed a complex biofilm structure comprising embedded MRSA in a self-produced extracellular matrix of EPS (Fig. 5B), which is contrary to planktonic bacteria shown in inset Fig. 5B. Confocal images also confirmed the formation of biofilm, as shown in Fig. 5C. SYTO-9 and TRITC were used to evaluate the viability of MRSA biofilms and optimized EPS matrix visualization. The green color in the inset figure represents bacterial colonies, whereas the red color represents the EPS matrix. SYTO 9 (green emission) stained all cells in the microbial population regardless of viability. TRITC (red emission) is a lectin-specific dye with high specificity for the mannose sugars present in EPS [64]. The formation of MRSA biofilms on wounds was macroscopically and microscopically confirmed. Based on these results, MRSA biofilm-infected wounds were used for further studies to evaluate the anti-biofilm and wound healing activities of the CS/NO film.

3.6. In vivo biofilm dispersal and wound healing activities

Next, we evaluated the *in vivo* wound healing effects of CS/NO film to accelerate the wound healing process in MRSA biofilm-infected wounds under the diabetic condition. Because MRSA biofilm infection also occurs under the non-diabetic condition, we examined the healing efficacy of the CS/NO film in non-diabetic ICR mice. Since a mouse is known as a loose-skinned animal, the elasticity of back skin can cause the reduction of the tension around wound, resulting in accelerated wound contraction [65]. To overcome the problem, Tegaderm™ was used to fix the skin to minimize the effect of wound contraction on wound healing [66]. The wounds were treated with the 0.8 cm × 0.8 cm (~15 mg) CS

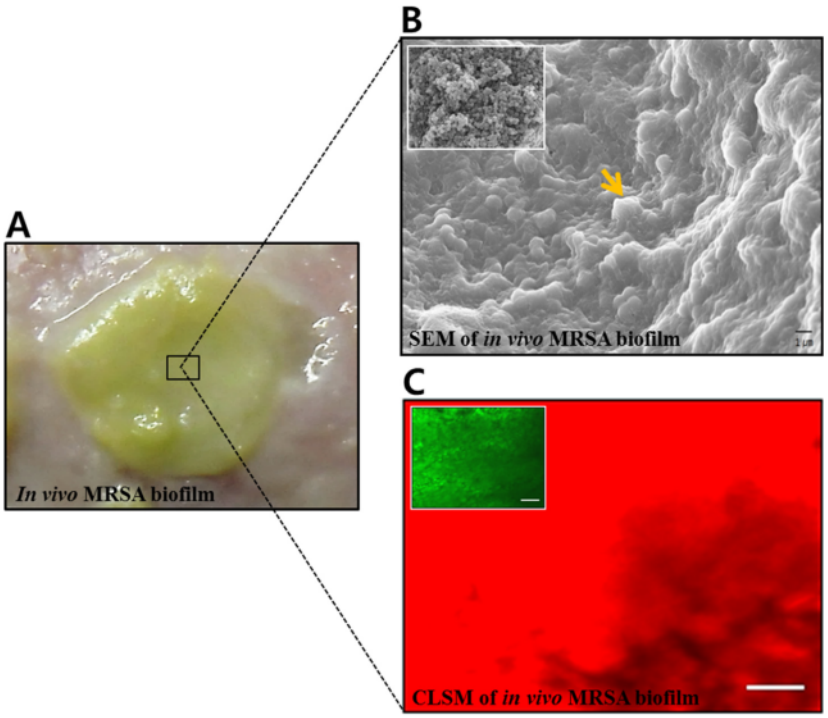

Fig. 5. Characterization of *in vivo* MRSA biofilm. (A) MRSA biofilm on wound. (B) SEM images of MRSA biofilm. Inset figure represents planktonic MRSA. (C) Confocal image of biofilm stained using tetramethylrhodamine isothiocyanate (TRITC). Inset figure represents planktonic MRSA stained using SYTO-9.

film and CS/NO film (3. 8 μmoles of NO/15 mg film) every 3 days; this interval was chosen based on the NO release profiles (Fig. 1B).

The macroscopic appearances of the wounds and percentage of wound area on different days are presented in Fig. 6. As shown in Fig. 6A, the CS film and CS/NO film treatment dispersed the MRSA biofilm, followed by enhanced wound healing under the non-diabetic and diabetic conditions; conversely, in the untreated group, neither the biofilm nor wound size were affected. In the CS film-treated groups, the *in vivo* MRSA biofilm dispersal was observed at day 15 post-injury in both non-diabetic and diabetic mice groups. Due to the combined effects of CS and NO, MRSA biofilm dispersal by the CS/NO film occurred faster than in the CS film-treated groups. The MRSA biofilm dispersal was observed at day 12 post-injury under the non-diabetic and diabetic conditions, followed by significant wound size reduction. The percentage of wound area of mice skin lesions comparative to the initial 6-mm wound is shown in Fig. 6B. The percentage of wound area in the CS film-treated groups observed on the last day (day 15 post-injury) was 31.8% ($P < 0.05$) and 40.6% ($P < 0.05$) under the non-diabetic and diabetic conditions, respectively. The wounds treated with CS/NO films showed faster re-epithelialization and closure compared to CS film-treated groups. The percentage of wound area observed at day 15 post-injury was 4.5% ($P < 0.05$) in the non-diabetic ICR mice and 5.8% ($P < 0.05$) in the STZ-induced diabetic ICR mice. In contrast to the CS film-treated group and CS/NO film-treated group, the untreated group showed visible biofilm growth with non-healing wounds up to day 15 post-injury under the both non-diabetic and diabetic conditions. These results prove that biofilm dispersal has a pivotal role in accelerating wound healing, which otherwise would result in severely delayed wound healing [67].

Both CS film-treated and CS/NO film-treated groups showed improved wound healing owing to their corresponding therapeutic activities. However, the CS/NO film accelerated wound healing more significantly than the CS film due to the synergistic wound healing activities of CS and NO. CS modulates the function of inflammatory cells (i.e., polymorphonuclear leukocytes, macrophages, and fibroblasts), resulting in granulation and cell migration [68–72]. NO is known to enhance wound healing by multiple mechanisms; such as by mediating inflammation-induced edema formation and keratonocyte proliferation, improving wound re-epithelialization, and promoting collagen formation [73]. Moreover, the film-based dressing of our system has several advantages for wound repair. First, it has high gas-permeability and low maceration and involves painless administration. Second, the film transparency enables easy wound monitoring. Lastly, it can prevent wound dehydration and contamination and can maintain a sterile wound exudate [54,74].

3.7. Histological analyses

Histological examinations of H&E and MT stained sections were performed to observe the progress of wound healing. Fig. 7A shows microscopic images under H&E and MT staining of normal mouse skin, untreated wound, and wound treated with CS and CS/NO films. H&E and MT staining were used to analyze skin morphology and collagen deposition, respectively. In the non-diabetic group, the untreated and CS film-treated groups showed open wounds and early epithelialization, ulceration, and abundance of mononuclear inflammatory cells with deep inflammatory infiltration through the dermal layer, whereas the CS/NO film-treated groups showed enhanced re-epithelialization and collagen deposition,

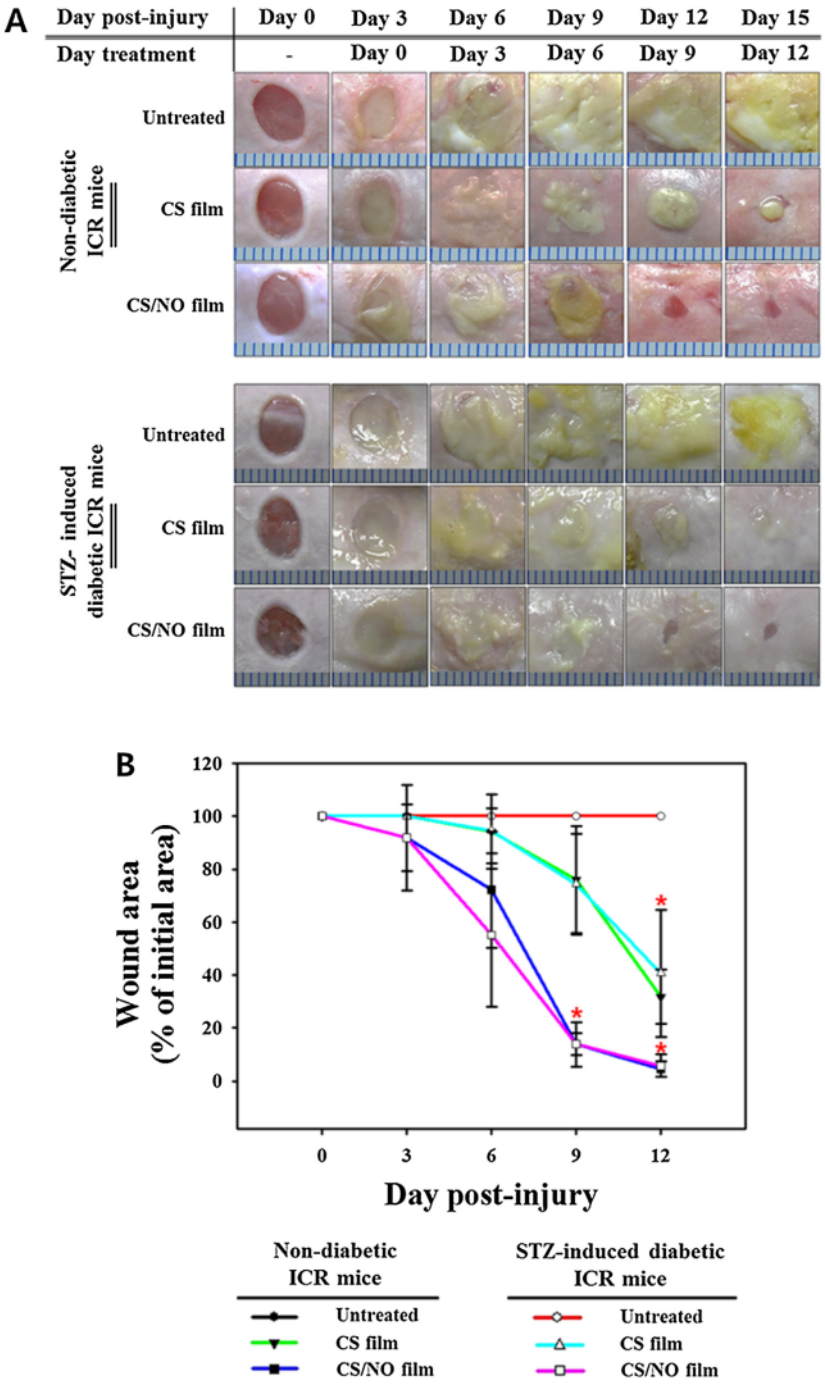

Fig. 6. MRSA biofilm-infected wounds in non-diabetic and STZ-induced diabetic ICR mice. (A) Representative photographs of healing in non-diabetic (upper panel) and STZ-induced diabetic ICR mice (lower panel) with MRSA biofilm challenge treated with or without the CS/NO film. (B) Wound area reduction percentage of mice skin lesions relative to the initial 6-mm wound. Data shown are mean ± SD (n = 6), different wounds; *P < 0.05, compared with untreated group.

similar to that observed in healthy mice skin tissues. Collagen fibers, which were not differentiable using H&E staining, could be clearly seen using MT staining represented by its blue color. The blue intensity on trichrome staining indicates collagen, which usually appears in the remodeling phase of wound healing arranged parallel to the surface. GSNO is reported to accelerate wound contraction and re-epithelialization by increasing the number of fibroblast cells and amount of mast cells and vessels and to

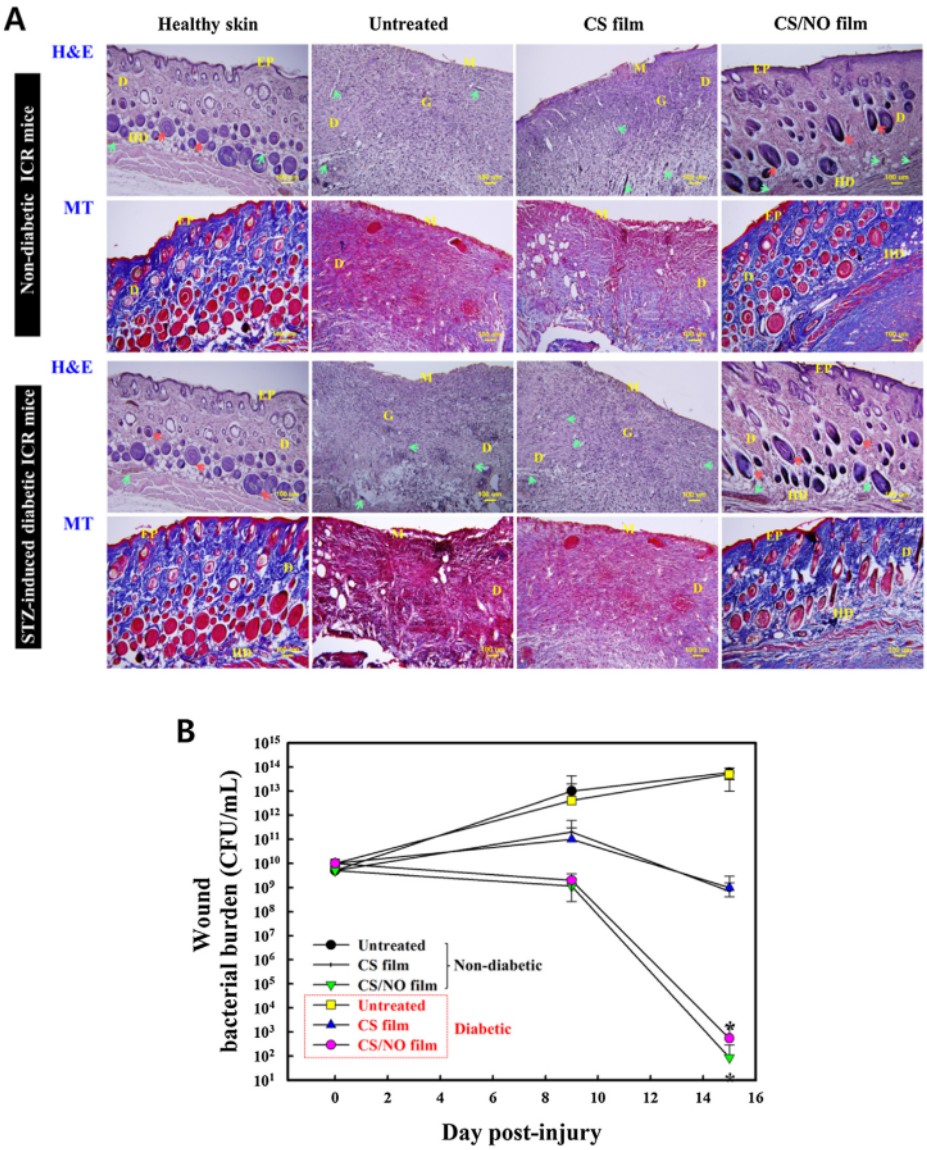

Fig. 7. (A) Histological analyses (H&E and MT staining) of MRSA biofilm-infected wounds in non-diabetic and STZ-induced diabetic ICR mice at day 15 post-injury (magnification 10×, scale bar = 100 μm); EP = epidermis; D = dermis; HD = hypodermis; M = wound matrix; G = granulation tissue. Orange arrows denote hair follicles and green arrows indicate blood vessles (capillaries and neovascularization). Blue colors in the MT staining images indicate collagen arranged parallel to the surface. (B) Bacterial viability (CFU/mL) on MRSA biofilm-infected wounds in non-diabetic and STZ-induced diabetic ICR mice. At day 9 and 15 post-injury, skin lesion tissues with biofilm were homogenized in sterile PBS and cultured onto TSB agar at 37 °C overnight.

trigger collagen deposition in cutaneous wound healing [75,76]. The histological results of the non-diabetic group did not differ from those in the diabetic group.

3.8. Reduction of bacterial burden on wounds

Lastly, for the effective treatment of MRSA biofilm-infected wounds, dispersal of biofilm on the wounds must be performed to accelerate wound healing. Moreover, the bacteria within the biofilm secrete virulence compounds which may hinder wound repair processes, including cell proliferation and migration [77,78]. Quantitative measurement of planktonic bacteria on wound tissues was used to observe the progress of biofilm dispersal and reduction of wound bacterial burden (Fig. 7B). Bacterial viability (CFU/mL) on MRSA biofilm-infected wounds was evaluated at day 9 and 15 post-injury in the non-diabetic and diabetic groups. As shown in Fig. 7B, in the untreated group, the number of bacteria that colonized the wound increased from day 6 to 15 post-injury. The CS film and CS/NO film-treated groups showed no significant reduction in wound bacterial burden at day 9 post-injury in the non-diabetic and diabetic ICR mice; the biofilm in the CS film-treated group tended to increase, whereas that in the

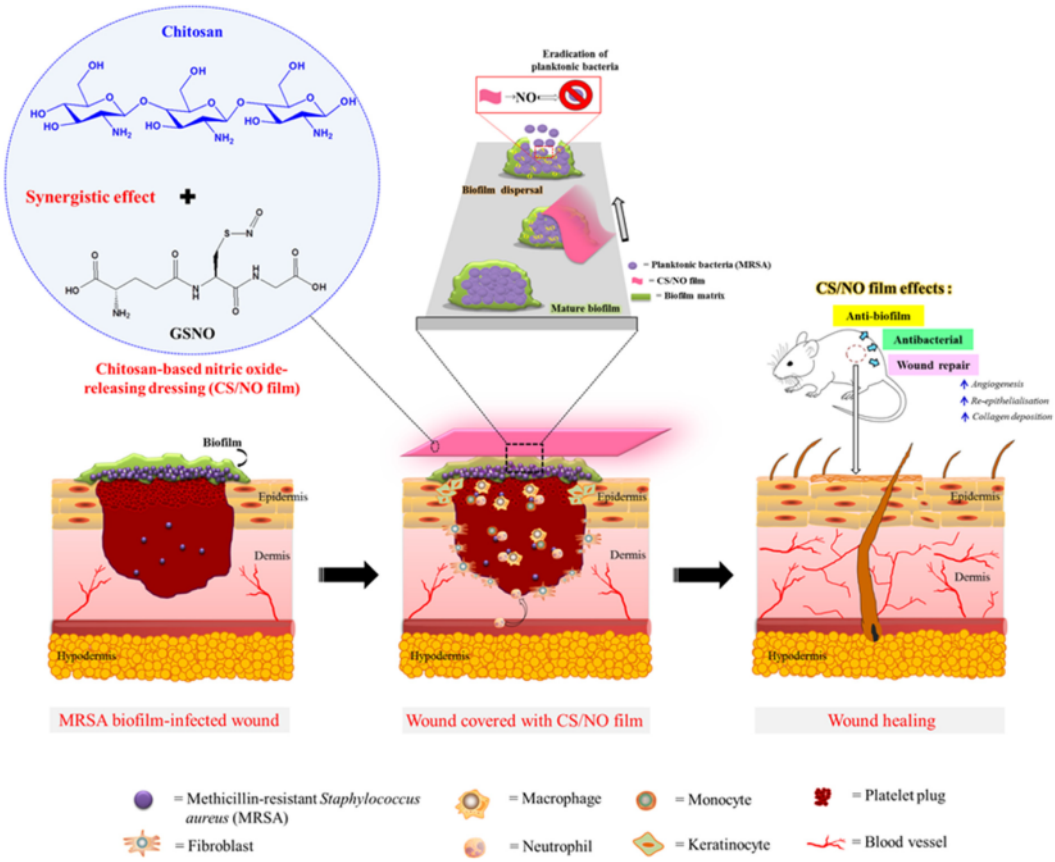

Fig. 8. Illustration of mechanisms of action of CS and GSNO in the CS/NO film in MRSA biofilm-infected wound healing.

CS/NO film-treated group it started to decrease. MRSA biofilm dispersal in the CS film-treated and CS/NO-treated groups began after day 9 post-injury. The CS film-treated group showed approximately ~ 2 log reduction (99% bacterial viability) from day 9 at day 15 post-injury in the non-diabetic and diabetic ICR mice. The CS/NO film showed more noticeable reduction in bacterial viability by > 6 logs (99.9999% bacterial viability) in day 15 post-injury in the non-diabetic and diabetic ICR mice. This result suggests that NO has biofilm dispersal and antibacterial properties. These dual activities showed significant results compared with those in other groups.

4. Conclusions

In this study, chitosan-based nitric oxide-releasing dressings (CS/NO film) were prepared, and their anti-biofilm and wound healing activities were evaluated in MRSA biofilm-infected wounds under the diabetic condition in a mouse model. The CS/NO film released NO in a sustained manner for over 3 days under the swollen and immersed conditions. In the *in vitro* antibacterial and anti-biofilm studies, the CS/NO film significantly decreased the bacterial viability and biofilm biomass of MRSA. Importantly, the CS/NO films enhanced wound healing in MRSA biofilm-infected wounds under the diabetic condition (Fig. 8). Therefore, the findings from this study provide strong evidence of the clinical applicability of the CS/NO films for successful wound treatment under complicated diseased conditions such as diabetes and wound infections.

Acknowledgments

This research was supported by a grant of the Korea Health Technology R&D Project through the Korea Health Industry Development Institute (KHIDI), funded by the Ministry of Health & Welfare, Republic of Korea (grant number : HI15C2558).

References

[1] P. Martin, Wound healing–aiming for perfect skin regeneration, Science 276 (1997) 75–81.
[2] L. Braiman-Wiksman, I. Solomonik, R. Spira, T. Tennenbaum, Novel insights into wound healing sequence of events, Toxicol. Pathol. 35 (2007) 767–779.
[3] S. Guo, L.A. DiPietro, Factors affecting wound healing, J. Dent. Res. 89 (2010) 219–229.
[4] K.A. Moran, C.K. Murray, E.L. Anderson, Bacteriology of blood, wound, and sputum cultures from non-US casualties treated in a combat support hospital in Iraq, Infect. Control 29 (2008) 981–984.
[5] V. Falanga, Wound healing and its impairment in the diabetic foot, The Lancet 366 (2005) 1736–1743.
[6] T. Bjarnsholt, K. Kirketerp-Møller, P.Ø. Jensen, K.G. Madsen, R. Phipps, K. Krogfelt, N. Høiby, M. Givskov, Why chronic wounds will not heal: a novel hypothesis, Wound Repair Regen. 16 (2008) 2–10.
[7] S.C. Davis, C. Ricotti, A. Cazzaniga, E. Welsh, W.H. Eaglstein, P.M. Mertz, Microscopic and physiologic evidence for biofilm-associated wound colonization in vivo, Wound Repair Regen. 16 (2008) 23–29.
[8] D.M. Morens, G.K. Folkers, A.S. Fauci, The challenge of emerging and re-emerging infectious diseases, Nature 430 (2004) 242–249.
[9] D. Mack, H. Rohde, S. Dobinsky, J. Riedewald, M. Nedelmann, J.K.-M. Knobloch, H.-A. Elsner, H.H. Feucht, Identification of three essential regulatory gene loci governing expression of Staphylococcus epidermidis polysaccharide intercellular adhesin and biofilm formation, Infect. Immun. 68 (2000) 3799–3807.

[10] R.D. Wolcott, D.D. Rhoads, S.E. Dowd, Biofilms and chronic wound inflammation, J. Wound Care 17 (2008) 333–341.
[11] C. Dang, Y. Prasad, A. Boulton, E. Jude, Methicillin-resistant *Staphylococcus aureus* in the diabetic foot clinic: a worsening problem, Diabetic Med. 20 (2003) 159–161.
[12] L.S. McKittrick, J.B. McKittrick, T.S. Risley, Transmetatarsal amputation for infection or gangrene in patients with diabetes mellitus, Ann. Surg. 130 (1949) 826.
[13] D. Rhoads, R. Wolcott, S. Percival, Biofilms in wounds: management strategies, J. Wound care 17 (2008) 502.
[14] M.A. Fischbach, C.T. Walsh, Antibiotics for emerging pathogens, Science 325 (2009) 1089–1093.
[15] G. Taubes, The bacteria fight back, Science (2008) 356–361.
[16] R. Scatena, P. Bottoni, A. Pontoglio, B. Giardina, Pharmacological modulation of nitric oxide release: new pharmacological perspectives, potential benefits and risks, Curr. Med. Chem. 17 (2010) 61–73.
[17] L.R. Martinez, G. Han, M. Chacko, M.R. Mihu, M. Jacobson, P. Gialanella, A.J. Friedman, J.D. Nosanchuk, J.M. Friedman, Antimicrobial and healing efficacy of sustained release nitric oxide nanoparticles against *Staphylococcus aureus* skin infection, J. Invest. Dermatol. 129 (2009) 2463–2469.
[18] N. Barraud, D. Schleheck, J. Klebensberger, J.S. Webb, D.J. Hassett, S.A. Rice, S. Kjelleberg, Nitric oxide signaling in *Pseudomonas aeruginosa* biofilms mediates phosphodiesterase activity, decreased cyclic di-GMP levels, and enhanced dispersal, J. Bacteriol. 191 (2009) 7333–7342.
[19] S. Schlag, C. Nerz, T.A. Birkenstock, F. Altenberend, F. Götz, Inhibition of staphylococcal biofilm formation by nitrite, J. Bacteriol. 189 (2007) 7911–7919.
[20] D.T. Efron, D. Most, A. Barbul, Role of nitric oxide in wound healing, Curr. Opin. Clin. Nutr. Metab. Care 3 (2000) 197–204.
[21] N. Hasan, J. Cao, J. Lee, M. Naeem, S.P. Hlaing, J. Kim, Y. Jung, B.-L. Lee, J.-W. Yoo, PEI/NONOates-doped PLGA nanoparticles for eradicating methicillin-resistant *Staphylococcus aureus* biofilm in diabetic wounds via binding to the biofilm matrix, Mater. Sci. Eng. C 103 (2019) 109741.
[22] K.S.B. Masters, S.J. Leibovich, P. Belem, J.L. West, L.A. Poole-Warren, Effects of nitric oxide releasing poly (vinyl alcohol) hydrogel dressings on dermal wound healing in diabetic mice, Wound Repair Regen. 10 (2002) 286–294.
[23] W.A. Seitz, R.E. Garfield, A.T. Balaban, R.J. Stewart, Systems and methods for topical treatment with nitric oxide, Google Patents, 2000.
[24] S.P. Hlaing, J. Kim, J. Lee, N. Hasan, J. Cao, M. Naeem, E.H. Lee, J.H. Shin, Y. Jung, B.-L. Lee, S-Nitrosoglutathione loaded poly (lactic-co-glycolic acid) microparticles for prolonged nitric oxide release and enhanced healing of methicillin-resistant *Staphylococcus aureus*-infected wounds, Eur. J. Pharm. Biopharm. 132 (2018) 94–102.
[25] S. Regmi, J. Cao, S. Pathak, B. Gupta, B.K. Poudel, P.T. Tung, S. Yook, J.-B. Park, C. S. Yong, J.O. Kim, A three-dimensional assemblage of gingiva-derived mesenchymal stem cells and NO-releasing microspheres for improved differentiation, Int. J. Pharm. 520 (2017) 163–172.
[26] J.O. Kim, J.-K. Noh, R.K. Thapa, N. Hasan, M. Choi, J.H. Kim, J.-H. Lee, S.K. Ku, J.-W. Yoo, Nitric oxide-releasing chitosan film for enhanced antibacterial and in vivo wound-healing efficacy, Int. J. Biol. Macromol. 79 (2015) 217–225.
[27] B. Wang, K. Chen, S. Jiang, F. Reincke, W. Tong, D. Wang, C. Gao, Chitosan-mediated synthesis of gold nanoparticles on patterned poly (dimethylsiloxane) surfaces, Biomacromolecules 7 (2006) 1203–1209.
[28] H. Yi, L.-Q. Wu, W.E. Bentley, R. Ghodssi, G.W. Rubloff, J.N. Culver, G.F. Payne, Biofabrication with chitosan, Biomacromolecules 6 (2005) 2881–2894.
[29] M. Burkatovskaya, G.P. Tegos, E. Swietlik, T.N. Demidova, A.P. Castano, M.R. Hamblin, Use of chitosan bandage to prevent fatal infections developing from highly contaminated wounds in mice, Biomaterials 27 (2006) 4157–4164.
[30] S. Manchanda, P.K. Sahoo, Fabrication and characterization of mucoadhesive topical nanoformulations of dorzolamide HCl for ocular hypertension, J. Pharm. Invest. 48 (2018) 323–332.
[31] M. Luangtana-anan, J. Nunthanid, S. Limmatvapirat, Potential of different salt forming agents on the formation of chitosan nanoparticles as carriers for protein drug delivery systems, J. Pharm. Invest. 49 (2019) 37–44.
[32] M.A. Oshi, M. Naeem, J. Bae, J. Kim, J. Lee, N. Hasan, W. Kim, E. Im, Y. Jung, J.-W. Yoo, Colon-targeted dexamethasone microcrystals with pH-sensitive chitosan/alginate/Eudragit S multilayers for the treatment of inflammatory bowel disease, Carbohydr. Polym. 198 (2018) 434–442.
[33] S.-H. Lim, S.M. Hudson, Review of chitosan and its derivatives as antimicrobial agents and their uses as textile chemicals, J. Macromol. Sci. Polym. Rev. 43 (2003) 223–269.
[34] M.A. Hassan, A.M. Omer, E. Abbas, W.M. Baset, T.M. Tamer, Preparation, physicochemical characterization and antimicrobial activities of novel two phenolic chitosan Schiff base derivatives, Sci. Rep. 8 (2018) 11416.
[35] E.M. Costa, S. Silva, F. Tavaria, M. Pintado, Insights into chitosan antibiofilm activity against methicillin-resistant *Staphylococcus aureus*, J. Appl. Microbiol. 122 (2017) 1547–1557.
[36] J.-W. Yoo, G. Acharya, C.H. Lee, In vivo evaluation of vaginal films for mucosal delivery of nitric oxide, Biomaterials 30 (2009) 3978–3985.
[37] B. Hakonen, L.K. Lönnberg, E. Larkö, K. Blom, A novel qualitative and quantitative biofilm assay based on 3D soft tissue, Int. J. Biomater. 2014 (2014), https://doi.org/10.1155/2014/768136.
[38] J.J. Harrison, M. Rabiei, R.J. Turner, E.A. Badry, K.M. Sproule, H. Ceri, Metal resistance in Candida biofilms, FEMS Microbiol. Ecol. 55 (2006) 479–491.
[39] B.L. Furman, Streptozotocin-induced diabetic models in mice and rats, Curr. Protoc. Pharmacol. 70 (2015) 5–47.
[40] K.M. Davies, D.A. Wink, J.E. Saavedra, L.K. Keefer, Chemistry of the diazeniumdiolates. 2. Kinetics and mechanism of dissociation to nitric oxide in aqueous solution, J. Am. Chem. Soc. 123 (2001) 5473–5481.
[41] G. Han, L.N. Nguyen, C. Macherla, Y. Chi, J.M. Friedman, J.D. Nosanchuk, L.R. Martinez, Nitric oxide–releasing nanoparticles accelerate wound healing by promoting fibroblast migration and collagen deposition, Am. J. Pathol. 180 (2012) 1465–1473.
[42] R.C. Goy, D. de Britto, O.B. Assis, A review of the antimicrobial activity of chitosan, Polímeros 19 (2009) 241–247.
[43] J. Qu, X. Zhao, Y. Liang, Y. Xu, P.X. Ma, B. Guo, Degradable conductive injectable hydrogels as novel antibacterial, anti-oxidant wound dressings for wound healing, Chem. Eng. J. 362 (2019) 548–560.
[44] X. Zhao, B. Guo, H. Wu, Y. Liang, P.X. Ma, Injectable antibacterial conductive nanocomposite cryogels with rapid shape recovery for noncompressible hemorrhage and wound healing, Nat. Commun. 9 (2018) 2784.
[45] X. Zhao, P. Li, B. Guo, P.X. Ma, Antibacterial and conductive injectable hydrogels based on quaternized chitosan-graft-polyaniline/oxidized dextran for tissue engineering, Acta Biomater. 26 (2015) 236–248.
[46] S. Takenaka, M. Iwaku, E. Hoshino, Artificial *Pseudomonas aeruginosa* biofilms and confocal laser scanning microscopic analysis, J. Infect. Chemother. 7 (2001) 87–93.
[47] H. Mellegård, S. Strand, B. Christensen, P. Granum, S. Hardy, Antibacterial activity of chemically defined chitosans: influence of molecular weight, degree of acetylation and test organism, Int. J. Food Microbiol. 148 (2011) 48–54.
[48] F.C. Fang, Perspectives series: host/pathogen interactions. Mechanisms of nitric oxide-related antimicrobial activity, J. Clin. Invest. 99 (1997) 2818–2825.
[49] S.-H. Chang, H.-T.V. Lin, G.-J. Wu, G.J. Tsai, pH Effects on solubility, zeta potential, and correlation between antibacterial activity and molecular weight of chitosan, Carbohydr. Polym. 134 (2015) 74–81.
[50] S.H. Yu, F.L. Mi, Y.B. Wu, C.K. Peng, S.S. Shyu, R.N. Huang, Antibacterial activity of chitosan–alginate sponges incorporating silver sulfadiazine: effect of ladder-loop transition of interpolyelectrolyte complex and ionic crosslinking on the antibiotic release, J. Appl. Polym. Sci. 98 (2005) 538–549.
[51] A. Çakmak, Y. Çirpanli, E. Bilensoy, K. Yorganci, S. Çaliş, Z. Saribaş, V. Kaynarog ̆lu, Antibacterial activity of triclosan chitosan coated graft on hernia graft infection model, Int. J. Pharm. 381 (2009) 214–219.
[52] S. Tin, K.R. Sakharkar, C.S. Lim, M.K. Sakharkar, Activity of Chitosans in combination with antibiotics in *Pseudomonas aeruginosa*, Int. J. Biol. Sci. 5 (2009) 153.
[53] F. Tamara, C. Lin, F.-L. Mi, Y.-C. Ho, Antibacterial effects of chitosan/cationic peptide nanoparticles, Nanomaterials 8 (2018) 88.
[54] E.A. Kamoun, E.-R.S. Kenawy, X. Chen, A review on polymeric hydrogel membranes for wound dressing applications: PVA-based hydrogel dressings, J. Adv. Res. 8 (2017) 217–233.
[55] S.G. Jones, R. Edwards, D.W. Thomas, Inflammation and wound healing: the role of bacteria in the immuno-regulation of wound healing, Int. J. Lower Extremity Wounds 3 (2004) 201–208.
[56] X. Zhang, P.L. Bishop, Biodegradability of biofilm extracellular polymeric substances, Chemosphere 50 (2003) 63–69.
[57] M. Maifreni, F. Frigo, I. Bartolomeoli, S. Buiatti, S. Picon, M. Marino, Bacterial biofilm as a possible source of contamination in the microbrewery environment, Food Control 50 (2015) 809–814.
[58] A. Asli, E. Brouillette, C. Ster, M.G. Ghinet, R. Brzezinski, P. Lacasse, M. Jacques, F. Malouin, Antibiofilm and antibacterial effects of specific chitosan molecules on *Staphylococcus aureus* isolates associated with bovine mastitis, PLoS One 12 (2017), https://doi.org/10.1371/journal.pone.0176988 e0176988.
[59] N. Barraud, M.J. Kelso, S.A. Rice, S. Kjelleberg, Nitric oxide: a key mediator of biofilm dispersal with applications in infectious diseases, Curr. Pharm. Des. 21 (2015) 31–42.
[60] J.B. Kaplan, Biofilm dispersal: mechanisms, clinical implications, and potential therapeutic uses, J. Dent. Res. 89 (2010) 205–218.
[61] Y. Kim, S.H. Kim, Released exopolysaccharide (r-EPS) produced from probiotic bacteria reduce biofilm formation of enterohemorrhagic *Escherichia coli* O157: H7, Biochem. Biophys. Res. Commun. 379 (2009) 324–329.
[62] T. Wong, J. McGrath, H. Navsaria, The role of fibroblasts in tissue engineering and regeneration, Br. J. Dermatol. 156 (2007) 1149–1155.
[63] L. Hall-Stoodley, J.W. Costerton, P. Stoodley, Bacterial biofilms: from the natural environment to infectious diseases, Nat. Rev. Microbiol. 2 (2004) 95.
[64] T.R. Neu, G.D. Swerhone, J.R. Lawrence, Assessment of lectin-binding analysis for in situ detection of glycoconjugates in biofilm systems, Microbiology 147 (2001) 299–313.
[65] S. Aarabi, K.A. Bhatt, Y. Shi, J. Paterno, E.I. Chang, S.A. Loh, J.W. Holmes, M.T. Longaker, H. Yee, G.C. Gurtner, Mechanical load initiates hypertrophic scar formation through decreased cellular apoptosis, The FASEB J. 21 (2007) 3250–3261.
[66] S.H. Bae, Y.C. Bae, S.B. Nam, S.J. Choi, A skin fixation method for decreasing the influence of wound contraction on wound healing in a rat model, Arch. Plast. Surg. 39 (2012) 457.
[67] D.G. Metcalf, P.G. Bowler, Biofilm delays wound healing: A review of the evidence, Burns Trauma 1 (2013) 5.
[68] H. Ueno, T. Mori, T. Fujinaga, Topical formulations and wound healing applications of chitosan, Adv. Drug Delivery Rev. 52 (2001) 105–115.
[69] J. Qu, X. Zhao, Y. Liang, T. Zhang, P.X. Ma, B. Guo, Antibacterial adhesive injectable hydrogels with rapid self-healing, extensibility and compressibility as wound dressing for joints skin wound healing, Biomaterials 183 (2018) 185–199.

[70] X. Zhao, H. Wu, B. Guo, R. Dong, Y. Qiu, P.X. Ma, Antibacterial anti-oxidant electroactive injectable hydrogel as self-healing wound dressing with hemostasis and adhesiveness for cutaneous wound healing, Biomaterials 122 (2017) 34–47.
[71] A. Ehterami, M. Salehi, S. Farzamfar, A. Vaez, H. Samadian, H. Sahrapeyma, M. Mirzaii, S. Ghorbani, A. Goodarzi, In vitro and in vivo study of PCL/COLL wound dressing loaded with insulin-chitosan nanoparticles on cutaneous wound healing in rats model, Int. J. Biol. Macromol. 117 (2018) 601–609.
[72] T.M. Tamer, K. Valachová, M.A. Hassan, A.M. Omer, M. El-Shafeey, M.S.M. Eldin, L. Šoltés, Chitosan/hyaluronan/edaravone membranes for anti-inflammatory wound dressing: in vitro and in vivo evaluation studies, Mater. Sci. Eng. C 90 (2018) 227–235.
[73] M.B. Witte, A. Barbul, Role of nitric oxide in wound repair, Am. J. Surg. 183 (2002) 406–412.
[74] T. Dai, M. Tanaka, Y.-Y. Huang, M.R. Hamblin, Chitosan preparations for wounds and burns: antimicrobial and wound-healing effects, Expert Rev. Anti-Infect. Ther. 9 (2011) 857–879.
[75] H.N. Achuth, S.M. Moochhala, R. Mahendran, W.T.L. Tan, Nitrosoglutathione triggers collagen deposition in cutaneous wound repair, Wound Repair Regen. 13 (2005) 383–389.
[76] T.P. Amadeu, A.B. Seabra, M.G. De Oliveira, A.M. Costa, S-nitrosoglutathione-containing hydrogel accelerates rat cutaneous wound repair, J. Eur. Acad. Dermatol. Venereol. 21 (2007) 629–637.
[77] R.J. Marano, H.J. Wallace, D. Wijeratne, M.W. Fear, H. San Wong, R. O'Handley, Secreted biofilm factors adversely affect cellular wound healing responses in vitro, Sci. Rep. 5 (2015) 13296.
[78] N. Hasan, J. Cao, J. Lee, S.P. Hlaing, M.A. Oshi, M. Naeem, M.-H. Ki, B.L. Lee, Y. Jung, J.-W. Yoo, Bacteria-targeted clindamycin loaded polymeric nanoparticles: effect of surface charge on nanoparticle adhesion to MRSA, antibacterial activity, and wound healing, Pharmaceutics 11 (2019) 236.

15th_Paper_Nurhasni_Hasan_IJBM_(2019).pdf

ORIGINALITY REPORT

24%	15%	27%	1%
SIMILARITY INDEX	INTERNET SOURCES	PUBLICATIONS	STUDENT PAPERS

PRIMARY SOURCES

1	test.dovepress.com Internet Source	5%
2	Chi Juan Ma, Yunfan He, Xiaoxuan Jin, Yuchen Zhang, Xiangdong Zhang, Yibao Li, Mimi Xu, Kaiyang Liu, Yao Yao, Feng Lu. "Light-regulated nitric oxide release from hydrogel-forming microneedles integrated with graphene oxide for biofilm-infected-wound healing", Materials Science and Engineering: C, 2021 Publication	5%
3	Kim, Jong Oh, Jin-Ki Noh, Raj Kumar Thapa, Nurhasni Hasan, Moonjeong Choi, Jeong Hwan Kim, Joon-Hee Lee, Sae Kwang Ku, and Jin-Wook Yoo. "Nitric oxide-releasing chitosan film for enhanced antibacterial and in vivo wound-healing efficacy", International Journal of Biological Macromolecules, 2015. Publication	5%
4	Nurhasni Hasan, Jiafu Cao, Juho Lee, Shwe Phyu Hlaing et al. "Bacteria-Targeted	4%

Clindamycin Loaded Polymeric Nanoparticles: Effect of Surface Charge on Nanoparticle Adhesion to MRSA, Antibacterial Activity, and Wound Healing", Pharmaceutics, 2019
Publication

5	www.ncbi.nlm.nih.gov Internet Source	1 %
6	zzdlab.com Internet Source	1 %
7	www.freepatentsonline.com Internet Source	1 %
8	Satiesh Kumar Ramadass, Lone Saquib Nazir, Ramar Thangam, Ramesh Kannan Perumal et al. "Type I collagen peptides and nitric oxide releasing electrospun silk fibroin scaffold: A multifunctional approach for the treatment of ischemic chronic wounds", Colloids and Surfaces B: Biointerfaces, 2019 Publication	1 %
9	pubs.rsc.org Internet Source	1 %
10	epdf.pub Internet Source	1 %
11	irep.ntu.ac.uk Internet Source	1 %

Exclude quotes	On	Exclude matches	< 1%
Exclude bibliography	On		